# Reaction Kinetics and Characteristics of Polyurethane/Clay Nanocomposites

**Dae Su Kim, Jin-Tae Kim, Won Bum Woo**

*Department of Chemical Engineering, Chungbuk National University, 12, Kaesin-dong, Cheongju, 361-763 Korea*

Received 2 March 2004; accepted 2 September 2004
DOI 10.1002/app.21616
Published online in Wiley InterScience (www.interscience.wiley.com).

**ABSTRACT:** The reaction behavior and physical properties of polyurethane (PU)/clay nanocomposite systems were investigated. Organically modified clay was used as nanofillers to formulate the nanocomposites. Differential scanning calorimetry was used to study the reaction behavior of the PU/clay nanocomposite systems. The reaction rate of the nanocomposite systems increased with increasing clay content. The reaction kinetic parameters of proposed kinetic equations were determined by numerical methods. The glass transition temperatures of the PU/clay nanocomposite systems increased with increasing clay content. The thermal decomposition behavior of the PU/clay nanocomposites was measured by using thermogravimetric analysis. X-ray diffractometer and transmission electronic microscope data showed the intercalation of PU resin between the silicate layers of the clay in the PU/clay nanocomposites. A universal testing machine was used to investigate the tensile properties of the PU/clay nanocomposites. © 2005 Wiley Periodicals, Inc. J Appl Polym Sci 96: 1641–1647, 2005

**Key words:** nanocomposites; polyurethane; clay, kinetics (polymer); structure

## INTRODUCTION

The importance of polyurethane (PU) as an industrial material is increasing because it has excellent abrasion resistance and shows properties of both elastomers and plastics.[1] However, poor heat resistance of conventional PU limits its applications.[2]

Various experiments aiming at improving both the thermal stability and the mechanical properties of PU have been conducted. One attempt to improve the thermal stability of PU involved the chemical modification of its structure by introducing thermally stable heterocyclic groups.[3,4] Another modification involved the use of clay to achieve nanocomposite formation.[5,6]

In the past decade, material scientists showed great interest in organic–inorganic hybridized nanocomposites. The applications of nanocomposites have dramatically improved the material properties of engineering plastics, rubbers, coatings, and adhesives.[7,8] The attractive improvements include heat resistance, barrier properties, and mechanical and electrical properties, which usually result from the synergistic effect between organic and inorganic components. The properties of polymer nanocomposites are affected a great deal by different nanoparticles. To achieve the expected improvement by adding nanoparticles, understanding how these nanoparticles influence the organic matrix is important.[9]

Polymer/clay nanocomposites have attracted much interest over a wide range of scientific and practical viewpoints since the development of nylon-6/clay nanocomposites by Toyota researchers.[10–12] They exhibited a dramatic increase of mechanical, thermal, and gas/liquid barrier properties[13,14] and unusual chemical and physical phenomena[15,16] that typically are not exploited by their conventional microcomposites. Thus, they may bring new opportunities in high technology and industrial applications. For example, Toyota Motor Co. has applied the nylon/clay nanocomposites to an automotive timing-belt cover.[17]

In this study, PU/clay nanocomposites were prepared by mixing various amounts of organically modified clay with PU resin. The reaction kinetics of the PU/clay nanocomposite systems were investigated and analyzed as a function of clay content in the nanocomposites. The dispersion of the nanoscale silicate layers of the clay in the PU matrix was investigated because the overall properties of the nanocomposites would be determined not only by clay content but also by the structure of the nanocomposites. The effects of clay content on the thermal and mechanical properties of the nanocomposites were analyzed.

## EXPERIMENTAL

### Materials

Toluene diisocyanate (TDI), having two functional isocyanate groups, was supplied by DC Chemical Co.

*Correspondence to:* D. S. Kim (dskim@chungbuk.ac.kr).

(Kunsan, Korea). The TDI was a mixture of 2,4-TDI (80%) and 2,6-TDI (20%). Poly(propylene glycol) (PPG), having three functional hydroxyl groups, was supplied by Kumho Petrochemical Co. (Ulsan, Korea). The molecular weight of the PPG was ~ 1000 g/mol.

Organically modified clay (Cloisite 30B) was supplied by Southern Clay Products Inc. (USA). The organic modifier used to produce the clay by modifying pristine clay was methyl tallow bis-2-hydroxyethyl quaternary ammonium ($MT_2EtOH$). The tallow in the modifier was predominantly an octadecyl chain with smaller amounts of lower homologues (approximate composition: ~ 65% C18; ~ 30% C16; ~ 5% C14). It was noteworthy that $MT_2EtOH$ has two hydroxyl groups. The modifier concentration in the clay was 90 meq/100 g of clay.

### Preparation of PU/clay nanocomposites

*In situ* intercalative polymerization technique was used to prepare PU/clay nanocomposites. Different amounts of the clay [1, 3, 5 phr (parts per hundred of PU resin)] was mixed with PPG and stirred at room temperature for 30 min to give enough time that the layered silicates could be swollen within PPG. Then, the mixture of clay and PPG was mixed with TDI by stoichiometry. The mixture was poured into a glass mold, after degassing it in a vacuum oven at room temperature. PU/clay nanocomposite film was obtained after curing the mixture in a dry oven at 100°C for 2.5 h.

### Measurements

#### Differential scanning calorimetry (DSC)

To obtain raw reaction kinetic data and investigate the reaction behavior of the PU/clay nanocomposite systems, DSC 2910 (TA Instruments, New Castle, DE) was employed. The samples for DSC were prepared according to the procedure described above. About 10 mg of the clay/PPG/TDI mixture was placed in a hermetic aluminum pan and tested immediately. The amount of the clay in the PU/clay nanocomposites was changed from 0 to 5 phr. Each sample was cured dynamically with different scanning rates of 5, 10, and 20°C/min under nitrogen gas flow (65 mL/min). The dynamic scanning temperature ranged from 10 to 200°C. Dynamic DSC second scans were performed to investigate the glass transition behavior of the nanocomposites at a scanning rate of 10°C/min.

#### Thermogravimetric analyzer (TGA)

To investigate the thermal degradation behavior of the PU/clay nanocomposites, thermogravimetric analysis was performed by using a TGA (SDT 2960, TA Instruments). Dynamic scanning was carried out from room temperature to 700°C at a scanning rate of 10°C/min under nitrogen gas flow (110 mL/min).

#### X-ray diffractometer (XRD)

XRD analysis was performed by using an XDS2000 X-ray diffractometer (Scintag Inc., Cupertino, CA) with CuK$\alpha$ radiation (wavelength = 0.15418 nm). The scanning speed was 2°/min and the step size was 0.02° in the range of 1.5°–10°.

#### Transmission electron microscope (TEM)

TEM images of the PU/clay nanocomposites were obtained by using the JEM-2011 (JEOL Ltd., Tokyo, Japan). A sample for TEM was prepared by placing a small portion of a PU/clay nanocomposite in an epoxy resin capsule and then curing the epoxy at 70°C for 2 h. The cured epoxy capsule impregnating a PU/clay nanocomposite was sliced by using a microtome (Leica Ultracut-R) into about 80-nm-thick slices at −30°C.

#### Universal testing machine (UTM)

Thin films were made by coating the PU/clay nanocomposite systems on glass plates and then curing, as described in the previous section. Tensile tests of the films were performed according to the ASTM D-882 by using a UTM (LR-30K, Lloyd Instruments, Hampshire, UK) at a crosshead speed of 50 mm/min. An average of at least five measurements was taken to report the tensile properties of the nanocomposite films. The dimension of the film specimens for tensile tests was 15 × 5 × 1 mm.

## RESULTS AND DISCUSSION

### Reaction kinetic analysis

The mechanisms of isocyanate reactions with active hydrogen compounds are still not completely understood because of their complexity. An example of the complexity of these reactions was shown in the mechanism proposed by Robins et al.[18] for metal ion catalyzed formation of urethanes. The reaction mechanism leads to a rate expression with an overall order which varies from 1 to 2 and first order with catalyst. Richter and Macosko[19] proposed a catalyst dissociation step which results in an order of 1/2–1 with catalyst.

The reaction kinetics of all urethane reactions may be described by the simplified kinetic expression

$$\frac{dC_{NCO}}{dt} = -kC_{cat}^{a}C_{NCO}^{b}C_{OH}^{c} \quad (1)$$

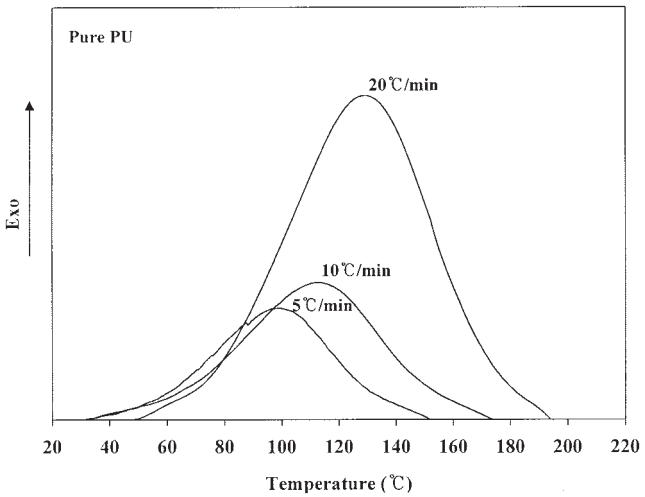


**Figure 1** Dynamic DSC thermograms of the pure PU system for various scanning rates.

where $a$ (=1/2–1) is the order with respect to catalyst, $b + c$ (=1–2) is the overall reaction order, and $C_{cat}$, $C_{NCO}$, and $C_{OH}$ are the concentrations of the catalyst, isocyanate, and active hydroxyl compound, respectively. This expression is not a mechanistic model. It has only one rate constant with a single activation energy to express a multitude of rates and equilibrium constants. The expression can be further simplified by lumping the catalyst concentration term into the rate constant.

Frequently it is considered that the isocyanate concentration is equal to the active hydroxyl concentration because most step polymerizations proceed near stoichiometry. Thus, the simplest expression used to describe the kinetics of urethane reaction is

$$\frac{dC}{dt} = -kC^n \tag{2}$$

where $n$ is mostly 2 under theoretical consideration (first order with isocyanate and first order with hydroxyl group). The parameter, $k$, was found to follow an Arrhenius dependence on temperature and could be described as

$$k = k_0 \exp\left(\frac{-E_a}{RT}\right) \tag{3}$$

where $k_0$ is frequency factor, $E_a$ is activation energy, and $R$ is the ideal gas constant.

The chemical conversion is defined as

$$\alpha = \frac{C_0 - C}{C_0} \tag{4}$$

where $C_0$ is initial concentration at time = 0 and $C$ is concentration at a certain reaction time.

By combining eqs. (1)–(4), a simple $n$th-order reaction kinetic equation can be obtained as[20]

$$\frac{d\alpha}{dt} = C_0 k_0 \exp\left(\frac{-E_a}{RT}\right)(1-\alpha)^n = A \exp\left(\frac{-E_a}{RT}\right)(1-\alpha)^n \tag{5}$$

By using the above kinetic equation, the reaction kinetics of the PU systems with or without clay was analyzed. The reaction kinetic parameters were determined by fitting experimental conversion data to the kinetic equation by using the Marquardt's multivariable nonlinear regression method and Runge–Kutta integration techniques.[21,22]

The experimental conversion data for reaction kinetic analysis were obtained from the dynamic DSC thermograms shown in Figure 1. The dynamic DSC thermograms for the pure PU system were obtained at various scanning rates. The peak temperature of each thermogram for maximum reaction heat evolution increased with an increasing scanning rate from 99 to 128°C. The peak temperature shift by scanning rate change depends on the activation energy associated with each reaction. Based on this peak-shifting phenomenon, there have been two methods discussed in the literature to calculate the activation energy associated with each reaction. They are Kissinger's method[23] and the method suggested by Ozawa[24] and Flynn.[25]

At first the overall reaction order [$n$ in eq. (5)] was fixed to 2 according to the theoretical consideration (first order with isocyanate and first order with hydroxyl group). Figure 2 shows fitting results by comparing the experimental conversion data obtained from the dynamic DSC thermograms with the conver-

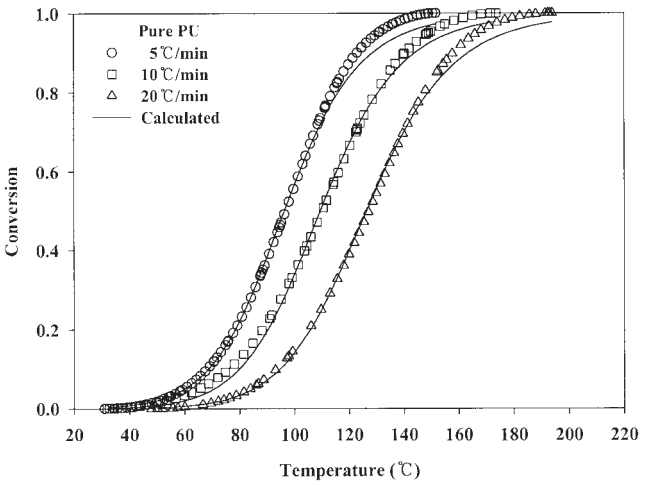


**Figure 2** Comparison of conversion changes measured from DSC (points) and calculated from the kinetic model (lines) for the pure PU system (second order).

**TABLE I**
**Values of Reaction Kinetic Parameters for the PU/Clay Systems**

| Clay content (phr) | $A$ (1/s) | $E_a$ (cal/mol) | $n$ |
|---|---|---|---|
| 0 | $2.99 \times 10^9$ | $1.86 \times 10^4$ | 2 (fixed) |
| 3 | $7.28 \times 10^9$ | $1.88 \times 10^4$ | 2 (fixed) |
| 0 | $5.14 \times 10^6$ | $1.42 \times 10^4$ | 1.35 (fitted) |
| 3 | $4.92 \times 10^7$ | $1.55 \times 10^4$ | 1.35 (fitted) |

sion curves fitted by the reaction kinetic equation with the overall reaction order of 2 for the pure PU system. Even though one dynamic DSC thermogram measured at a scanning rate is enough to determine reaction kinetic parameters by fitting, three DSC thermograms were used in this work because more experimental data would result in more accurate and reasonable kinetic parameters through the fitting process. The reaction kinetic parameters ($k_0$, $E_a$) for pure and clay-filled PU systems are listed in Table I. The fitting was fairly good in the low conversion range of under 0.7. However, the fitting was not so good in the high conversion range of over 0.7. The clay (3 phr)-filled PU system was also analyzed by the second-order kinetic equation. The trend of its fitting was almost similar to the pure PU system.

Therefore, the overall reaction order was not fixed to 2. It was also fitted through the fitting process as other kinetic parameters such as $A$ and $E_a$. The best-fit overall reaction order was 1.35 for the pure PU system. The reaction kinetic parameters ($k_0$, $E_a$, and $n$) for pure PU systems are listed in Table I. The fitting results are shown in Figure 3, which shows that the experimental conversion data obtained from the dynamic DSC thermograms were fitted well by the $n$th-order reaction kinetic equation for the pure PU system. Compared to the fitting shown in Figure 2, the fitting was pretty good, even in the high conversion range.

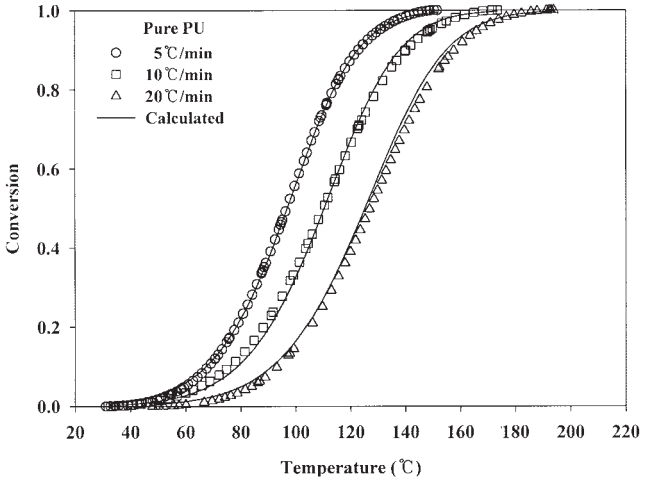


**Figure 3** Comparison of conversion changes measured from DSC (points) and calculated from the kinetic model (lines) for the pure PU system ($n$th order).

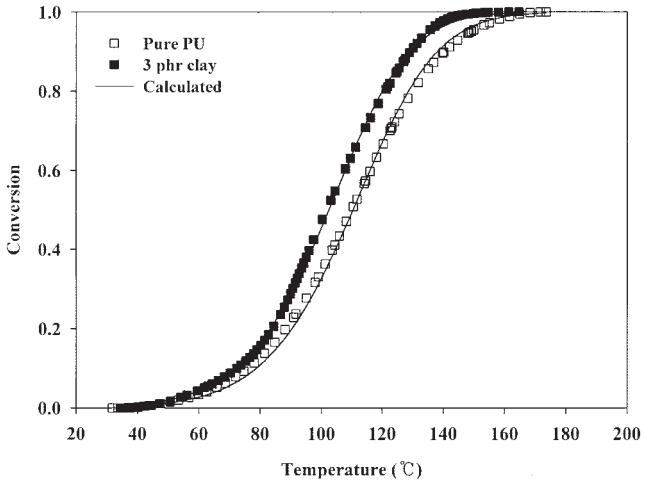


**Figure 4** Comparison of conversion changes measured from DSC (points) and calculated from the kinetic model (lines) for the pure and clay-filled 3 phr clay PU systems ($n$th order).

Figure 4 shows the conversion data obtained from the dynamic DSC thermograms and the conversion curves fitted by the $n$th-order reaction kinetic equation for pure and clay (3 phr)-filled PU systems. Similar to the pure PU system, the fitting results for the clay-filled PU system were also good. The best-fit overall reaction order was 1.35 for the clay-filled PU system. The reaction rate was increased considerably by the incorporation of the clay. It was considered that the clay played a role as a catalyst. The reaction kinetic parameters ($k_0$, $E_a$, and $n$) for the pure and clay-filled PU systems are listed in Table I.

## Thermal properties

The glass transition temperatures of the PU/clay nanocomposites containing different amounts of the clay were measured by using DSC at a scanning rate of 10°C/min as shown in Figure 5. The glass transition temperature of the nanocomposites increased very slightly with increasing clay content. From this result, it was considered that the clay was not sufficiently intercalated or exfoliated in the PU matrix.

Figure 6 shows TGA thermograms of the PU/clay nanocomposites containing different amounts of the clay. The 5% weight-loss temperature of the PU/clay nanocomposites increased with increasing clay content. The increase was 10°C for the nanocomposite containing 5 phr of the clay in comparison with pure PU. This increase in the thermal stability could be attributed to the high thermal stability of the clay and

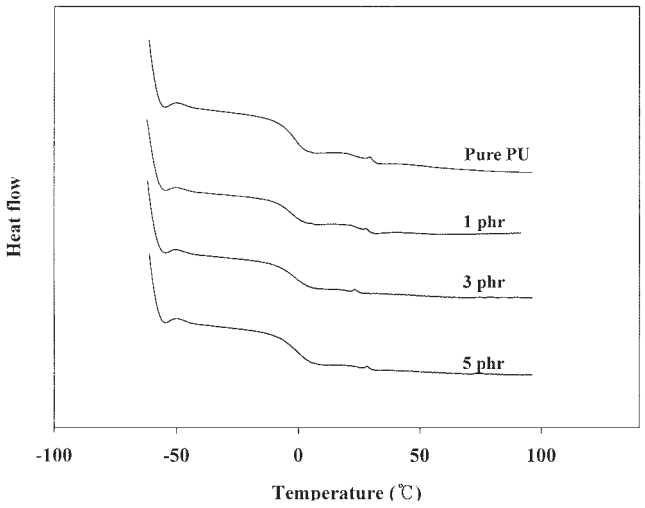


**Figure 5** Glass transitions of the PU/clay nanocomposite systems with various clay contents (scanning rate = 10°C/min).

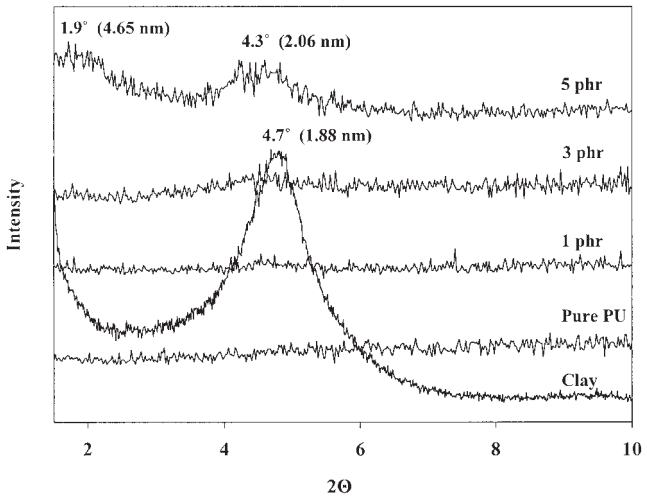


**Figure 7** XRD patterns of the PU/clay nanocomposite systems with various clay contents.

the interaction between the clay particles and the PU matrix.

### Structural analysis

XRD curves of the clay and PU/clay nanocomposites containing different amounts of the clay are shown in Figure 7. The XRD curve for the clay showed a characteristic diffraction peak at $2\theta = 4.7°$. Based on the Bragg equation, the *d*-spacing between the silicate layers of the clay is 1.88 nm. However, the main characteristic peak of the PU/clay nanocomposite containing 5 phr of the clay appeared at $2\theta = 4.3°$, corresponding to the *d*-spacing of 2.06 nm. Also, the secondary diffraction peak appeared at $2\theta = 1.9°$, corresponding to the *d*-spacing of 4.65 nm. In the case of the PU/clay nanocomposite containing 3 phr of the clay, the main characteristic peak appeared at about $2\theta = 4.3°$, but the secondary peak did not appear at about $2\theta = 1.9°$. In the PU/clay nanocomposites containing 3 or 5 phr of clay, the main peak is obviously the clay itself. This indicates that the silicate layers of the clay were partly intercalated and not homogeneously exfoliated in the PU matrix. No noticeable diffraction peak was observed for the nanocomposite containing 1 phr of the clay. This is considered to be due to too small an amount of the clay in the nanocomposite.

A TEM micrograph of the PU/clay nanocomposites containing 5 phr of the clay is shown in Figure 8. Although XRD is by far the simplest method available to measure the *d*-spacing of polymer nanocomposites, TEM has been also used to visually evaluate the degree of intercalation, exfoliation, and aggregation of clay clusters. The two representative regions marked as "little intercalation" and "large intercalation" in Figure 8 correspond to the two characteristic XRD peaks of the PU/clay nanocomposite containing 5 phr of the clay. TEM analysis supported the findings from XRD as well as showed visually that the clay was partly intercalated in two levels and not homogeneously exfoliated in the PU matrix.

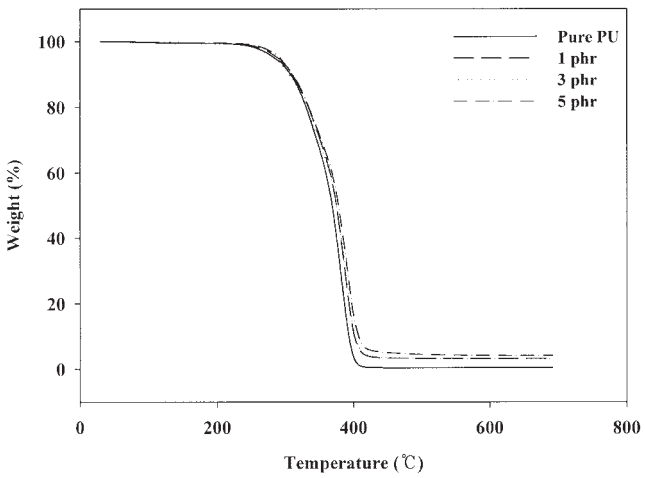


**Figure 6** Weight changes of the PU/clay nanocomposite systems with various clay contents (scanning rate = 10°C/min).

### Mechanical properties

The effect of clay content on the tensile strength of the nanocomposite is shown in Figure 9. The tensile strength of the PU/clay nanocomposite increased with increasing clay content. When the clay content was 5 phr, the tensile strength of the PU/clay nanocomposite was three times higher compared to that of pure PU. This enhancement of the tensile strength is

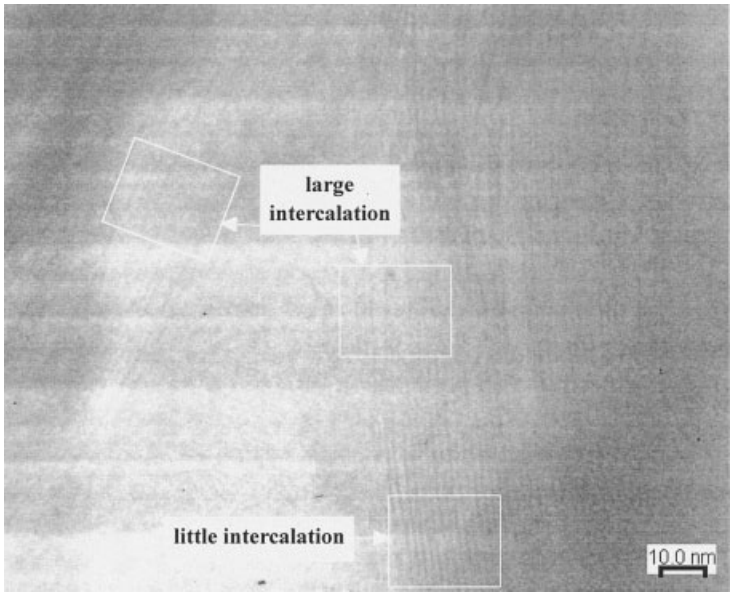


**Figure 8** TEM micrograph of the PU/clay nanocomposite system (5 phr).

ascribed to the resistance exerted by the clay itself as well as the orientation and aspect ratio of the clay layers. It is particularly noteworthy that the intercalated morphology shown in Figure 8 would affect positively in enhancing the tensile strength of the nanocomposite.

## CONCLUSIONS

The second-order kinetic equation derived theoretically could not describe well the reaction kinetics of the PU and PU/clay nanocomposite, especially in the high conversion range. The reaction kinetics of the PU and nanocomposite, however, could be described well by the *n*th-order kinetic equation. The overall reaction order for the PU and nanocomposite determined by best fitting was 1.35. The reaction kinetic parameters were determined by fitting the dynamic DSC conversion data to the kinetic equation. The reaction rate of the nanocomposite system was faster than pure PU system. The glass transition temperature of the PU/clay nanocomposites increased slightly with increasing clay content. The thermal stability of the PU/clay nanocomposites increased slightly with increasing clay content. XRD data for the nanocomposite showed peaks due to the intercalation of the PU between the silicate layers of the clay. A TEM micrograph showed similar results to the XRD results. The tensile strength of the nanocomposites increased with increasing clay content.

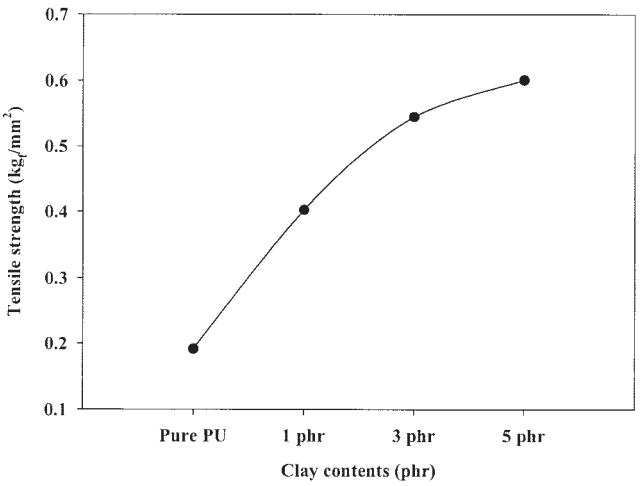


**Figure 9** Effects of clay content on the tensile strength of the PU/clay nanocomposites.

## References

1. Comstock, M. J. Urethane Chemistry and Applications; ACS Symposium Series 172; American Chemical Society: Washington, DC, 1981, Chapter 1.
2. Frisch, K. C.; Klempner, D. Advances in Urethane Science and Technology; Technomic Publishing: New York, 2001.
3. Masiulanis, B.; Zielinski, R. J Appl Polym Sci 1985, 30, 2731.
4. Wang, Z.; Pinnaviaia, T. J. Chem Mater 1998, 10, 3769.
5. Tien, Y. I.; Wei, K. H. Polymer 2001, 42, 3213.
6. Zilg, C.; Thomann, R.; Mulhaupt, R.; Finter, J. Adv Mater 1999, 11, 49.
7. Liu, L. M.; Qi, Z. N.; Zhu, X. G. J Appl Polym Sci 1999, 71, 1133.
8. Huang, H. H.; Wilkes, G. L.; Carlson, J G. Polymer 1989, 30, 2001.
9. Zhou, S.; Wu, L.; Sun, J.; Shen, W. Progr Org Coatings 2002, 45, 33.
10. Kawasumi, M.; Hasegawa, N.; Kato, M.; Usuki, A.; Okada, A. Macromolecules 1997, 30, 6333.
11. Usuki, A.; Kato, M.; Okada, A.; Kurauchi, T. J Appl Polym Sci 1997, 63, 137.

12. Hasegawa, N.; Kawasumi, M.; Kato, M.; Usuki, A.; Okada, A. J Appl Polym Sci 1998, 67, 87.
13. Kurokawa, Y.; Yasuda, H.; Kashiwagi, M.; Oya, A. J Mater Sci Lett 1997, 16, 1670.
14. Oya, A.; Kurokawa, Y.; Yasuda, H. J Mater Sci 2000, 35, 1045.
15. D'yachkovskii, F. S.; Novokshonaova, L. A. Russ Chem Rev 1984, 53, 117.
16. D'yachkovskii, F. S. Trends Polym Sci 1993, 1, 274.
17. Calvert, P. Nature 1996, 383, 300.
18. Robins, J.; Edwards, B. H.; Tokach, S. K. Adv Urethane Sci Technol 1984, 9, 65.
19. Richter, E. B.; Macosko, C. W. Polym Eng Sci 1978, 18, 1012.
20. Macosko, C. W. RIM Fundamentals of Reaction Injection Molding; Hanser Publishers: Munich Vienna New York, 1989; Chapter 2.
21. Kuester, J L.; Mize, J. M. Optimerization techniques with FORTRAN; McGraw-Hill: New York, 1973.
22. Kim, D. S.; Lee, S. K. J Appl Polym Sci 2001, 82 1952.
23. Kissinger, H. E. Anal Chem 1957, 29, 1706.
24. Ozawa, T. J. J Therm Anal 1976, 9, 217.
25. Flynn, J H. Therm Acta 1980, 37, 225.